Environmental Earth Sciences (2019) 78:170
https://doi.org/10.1007/s12665-019-8177-4

ORIGINAL ARTICLE

Climatic and environmental signals recorded in the EGRIP snowpit, Greenland

Zhiheng Du[1] · Cunde Xiao[2] · Qi Zhang[3] · Chuanjin Li[1] · Feiteng Wang[1] · Ke Liu[4] · Xiangyu Ma[1]

Received: 3 May 2018 / Accepted: 19 February 2019 / Published online: 27 February 2019

Abstract

Polar ice sheets conserve atmospheric mineral dust (aerosols) at the time of snowfall, and this material can be used to reconstruct historical climate and environmental conditions. Snowpit samples were obtained from the East Greenland Ice Core Project (EGRIP) site in July 2017. Mineral dust concentrations as well as stable water isotope ($\delta^{18}O$, δD, and deuterium excess) and major ion (F^-, Cl^-, NO_2^-, NO_3^-, SO_4^{2-}, methanesulfonic acid (MSA), Na^+, NH_4^+, Mg^{2+} and Ca^{2+}) concentrations were analyzed in this study. The seasonal $\delta^{18}O$ and δD cycles indicate that the snowpit samples covered the period from winter 2012 to summer 2017. The concentrations of mineral dust and Ca^{2+} showed seasonal deposition events with maxima in the spring layers. The concentrations of MSA exhibited maxima in the summer layers, making them useful indicators for the summer season. Moreover, an anomalous non-sea salt SO_4^{2-} (nss SO_4^{2-}) event was recorded at a depth of 130 – 85 cm that corresponded to the Holuhraun eruption (31 August 2014). In addition, a significant short-term cooling effect was observed. A back-trajectory analysis suggests that a major ash event from Iceland contributed to the Greenland ice sheet (GrIS). These results provide insight for future studies of the EGRIP ice core.

Keywords Mineral dust · Major ions · Environmental signal · Holuhraun eruption · East GRIP

Introduction

Ice core chemistry studies from the Greenland and Antarctic ice sheets have provided important information on the historical atmospheric chemistry over various time periods, including the industrial and preindustrial eras and the last glacial cycle (Legrand and Mayewski 1997). In the Arctic, impurities in the atmosphere and cryosphere can strongly affect the atmospheric radiation and surface energy balance (Groot Zwaaftink et al. 2016). Several studies have analyzed the impurities, chemical compositions and pollutants in ice cores from the GrIS and provided information about historical climate and environmental changes (McConnell and Edwards 2008; Steffensen 1997; Mayewski et al. 1993). A significant negative correlation has been observed between dust flux and temperature records during glacial periods, which can be attributed to a strengthening of dust transport patterns (Fischer et al. 2007; Ruth et al. 2003; Biscaye et al. 1997). For example, dust concentration profiles are consistent with the GISP2, GRIP, NGRIP and NEEM ice cores (Oyabu et al. 2015; Ruth et al. 2003; Fuhrer et al. 1999; Ram et al. 1997). These results revealed that mineral dust was a primary factor that controlled the climatic variations during the last glacial–interglacial cycle.

Volcanic eruptions are an important natural cause of climate change on different timescales. The energy of these blasts is sufficient to inject megatons of material directly into the upper atmosphere (Robock 2000). Large and powerful volcanic eruptions inject sulfur gases and ash into the stratosphere. The ash and pyroclastic materials fall rapidly to the ground due to gravity, but the gases remain in the atmosphere over longer timescales. These materials are

✉ Zhiheng Du
duzhiheng10@163.com

1 State Key Laboratory of Cryospheric Science, Northwest Institute of Eco-Environment and Resources, Chinese Academy of Sciences, Lanzhou 730000, China

2 State Key Laboratory of Land Surface Processes and Resource Ecology, Beijing Normal University, Beijing 100875, China

3 Institute of Climate System, China Meteorology Administration, Chinese Academy of Meteorological Science, Beijing 100081, China

4 School of Geographic and Oceanographic Sciences, Nanjing University, Nanjing, China

transported by atmospheric circulations and deposited on polar ice sheets. Among the gases derived from these events, SO_2 is of particular interest due to its conversion to small sulfuric acid aerosols, which can potentially impact the radiative budget of the atmosphere at the global scale (Williams et al. 2009; Ambrose 1998). However, the effects of historic eruptions on climate can also be preserved in ice cores and assessed using non-sea salt SO_4^{2-} (nss SO_4^{2-}) concentrations (Sigl et al. 2013; Cole-Dai et al. 2009; Larsen et al. 2008).

The East Greenland Ice Core Project (EGRIP), which is an international ice coring project led by the University of Copenhagen in Denmark, explores the climatic and ice sheet variations in Greenland. In 2017, we excavated one snowpit with a depth of 2.0 m at the EGRIP site (75°37′N, 35°59′W, 2702 m asl) to examine the seasonal variations of major ion species in the snow samples, which will be beneficial to study depth ice core in future. Snow sampling was carried out at 5-cm intervals in this snowpit, and a total of 40 snow samples were analyzed for concentrations of dust and ions, including Na^+, NH_4^+, Mg^{2+}, Ca^{2+}, F^-, Cl^-, NO_2^-, NO_3^-, SO_4^{2-} and CH_3SO_3-methanesulfonic acid (MSA), and stable isotopes of snow melt water ($\delta^{18}O$ and δD).

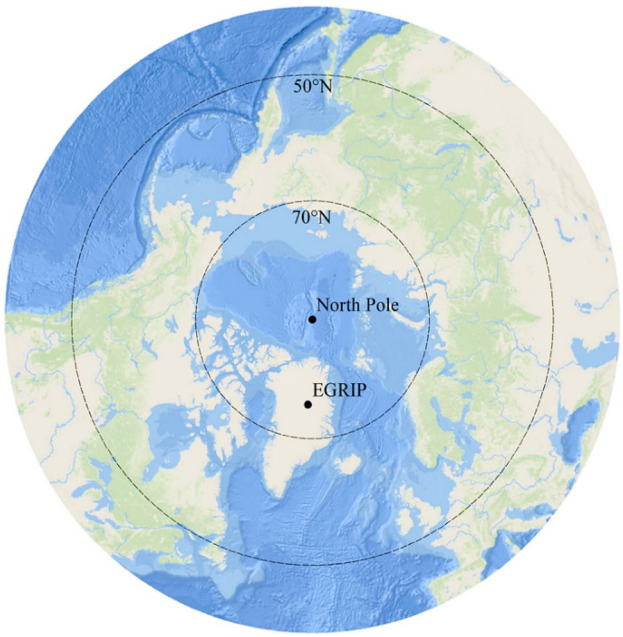

Fig. 1 Map of the snowpit site at the EGRIP site

Experimental section

Snowpit sample collection and preparation

A 2.0-m snowpit was excavated at the EGRIP site in East Greenland in June 2017 (Fig. 1). The reconstruction of the annual layer thickness from the 67-m shallow ice core at the EGRIP site indicated that the accumulation rate was 0.11 m/year (ice equivalent). Then, the snow samples were frozen and transported to the State Key Laboratory of Cryospheric Science (SKLCS) in July 2017. A total of 40 samples with a 5-cm resolution were analyzed for stable water isotopes, including oxygen ($\delta^{18}O$) and hydrogen (δD) isotope, using a Picarro L1102-i wavelength-scanned cavity ring-down spectrometer (Picarro Inc., USA) in SKLCS. In addition, the ion and dust concentrations of the samples were measured via ion chromatography (Dionex 3000) and an Accusizer 780A counter (PSS Corporation), respectively, at the SKLCS in Lanzhou, China.

Measurement method

The major ions, i.e., Na^+, NH_4^+, Mg^{2+} and Ca^{2+} as well as F^-, MSA, NO_2^-, Cl^-, NO_3^- and SO_4^{2-}, were analyzed via IC at SKLCS. The polypropylene vials were triple-rinsed with ultra-pure water (Milli-Q, > 18.2 MΩ) and ultrasonically cleaned for 30 min. This processing was repeated three times, and the major ion contents of the Milli-Q water were below the detection limits. The vials were dried for 2–3 h at 50 °C before use. Once the samples had melted in closed LDPE bottles at room temperature (20 °C) at SKLCS, the liquid samples were transferred into cleaned polypropylene vials, and the concentrations of ions were analyzed. The CS-12A and AS-11HC columns and CG-12A and AG-11HC guards were used for the analysis of cations and anions, respectively. A volume of 1 ml was injected, and then an isocratic analysis was performed for cations and a gradient analysis was performed for anions (Li et al. 2014). Blanks were measured alongside the analyzed samples, and the average blanks of Na^+, NH_4^+, Mg^{2+} and Ca^{2+}, F^-, MSA, NO_2^-, Cl^-, NO_3^- and SO_4^{2-}were 0.46 ng/g, 3.27 ng/g, 0.16 ng/g, 0.91 ng/g, 0.08 ng/g, 0.001 ng/g, 1.19 ng/g, 0.99 ng/g and 1.81 ng/g, respectively. The analytical errors determined from replicate measurements of chemical standards were within 5% of the average concentrations measured in the samples. The isotopic ratios were expressed in per mil (‰) using $\delta^{18}O$ and δD values relative to the Vienna Standard Mean Ocean Water (V-SMOW). The samples were measured on a Picarro L1102-i cavity ring-down spectrometer (CRDS) using the high-throughput Picarro-A0212 vaporizer. The results were calibrated with Vienna Standard Mean Ocean Water (VSMOW) and normalized to the VSMOW–SLAP (Standard Light Antarctic Precipitation) scale using $\delta^{18}O_{VSMOW} = 0.0‰$, $\delta^{18}O_{SLAP} = -55.5‰$, $\delta D_{VSMOW} = 0.0‰$ and $\delta D_{SLAP} = -427.5‰$. Note that this approach implies the use of a fixed two-point calibration line. We used three in-house standards with well-calibrated $\delta^{18}O$ and δD values with respect to the primary IAEA (International Atomic Energy Agency) standard

waters. Two of the in-house standards were used to estimate the two-point calibration line, and the third standard was used for quality control. The overall precision of the system was determined to be greater than 0.1‰ for $\delta^{18}O$ and greater than 0.5‰ for δD. Each sample measurement was repeated six times, and the average value was calculated. The 1σ reproducibilities were 0.02‰ for δD and 0.07‰ for $\delta^{18}O$. The procedure for analyzing dust concentrations and size distributions was adopted from previous studies with minor modifications (Dong et al. 2016). The preparation and analysis of the samples was conducted in a class 100 clean room at SKLCS. The measurement of the particle size distribution of the snow samples was performed in a class 100 clean hood using an Accusizer 780A counter, which uses the single-particle optical sensing (SPOS) method and is equipped with a 120 orifice. Size data were acquired for the range of 0.57–400 μm equivalent spherical diameters. Background counts were subtracted from the sample data. All samples were analyzed in random order and in triplicate. The results were then averaged for individual samples, yielding an estimated error of 10% or less for particle concentrations (Dong et al. 2016).

Results

Dating of the snowpit samples

Figure 2 shows the vertical profiles of the stable water isotopes ($\delta^{18}O$ and δD) and the excess deuterium (D-excess = $\delta D - 8\delta^{18}O$) of the samples from the EGRIP snowpit. Seasonal variations in the $\delta^{18}O$ and δD values were clearly observed in the depth profile and indicated that the snow in the 2.0-m pit was deposited from 2012 to 2017. The $\delta^{18}O$ and δD values reached their minima during winter. The $\delta^{18}O$ values varied between −45.00 and −28.84‰, with a mean value of 34.76‰ (Fig. 2). These results are similar to the mean annual $\delta^{18}O$ composition (−36.51‰) observed for a 67-m firn core drilled at the same location in 2012 (Vallelonga et al. 2014). In addition, the range of the δD values was −361.32 to −226.97‰, with a mean value of −271.35‰. The D-excess was characterized by values ranging between −0.48 and 11.25‰, with a mean value of 6.77‰. The $\delta^{18}O$ and δD depth profiles fluctuated in phase and recognizable seasonal patterns observed from Fig. 2. Because both $\delta^{18}O$ and δD are strongly correlated with temperature, the maximum and minimum $\delta^{18}O$ and δD values were observed in summer 2016 and winter 2017, respectively.

Seasonal variations in mineral dust and ion concentrations

The concentrations of insoluble dust in snow depend on the primary supply from a source region via long-range atmospheric transport as well as depositional processes, and the particle and mass concentration of mineral dust in snow can be linked to climate variability (Drab et al. 2002). The vertical profiles of dust particle numbers and anions (Na^+, NH_4^+, Mg^{2+} and Ca^{2+}) are shown in Fig. 3. Seasonal variations in

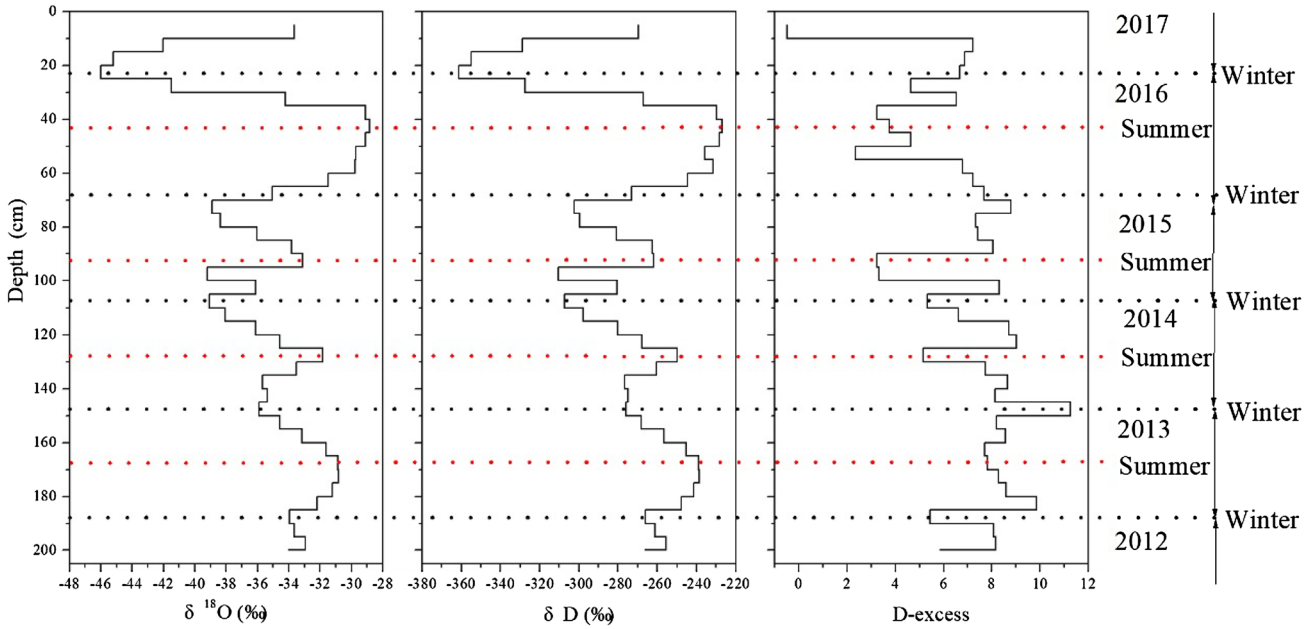

Fig. 2 Vertical profiles of stable water isotopes and D-excess (dashed black lines represent winter layers)

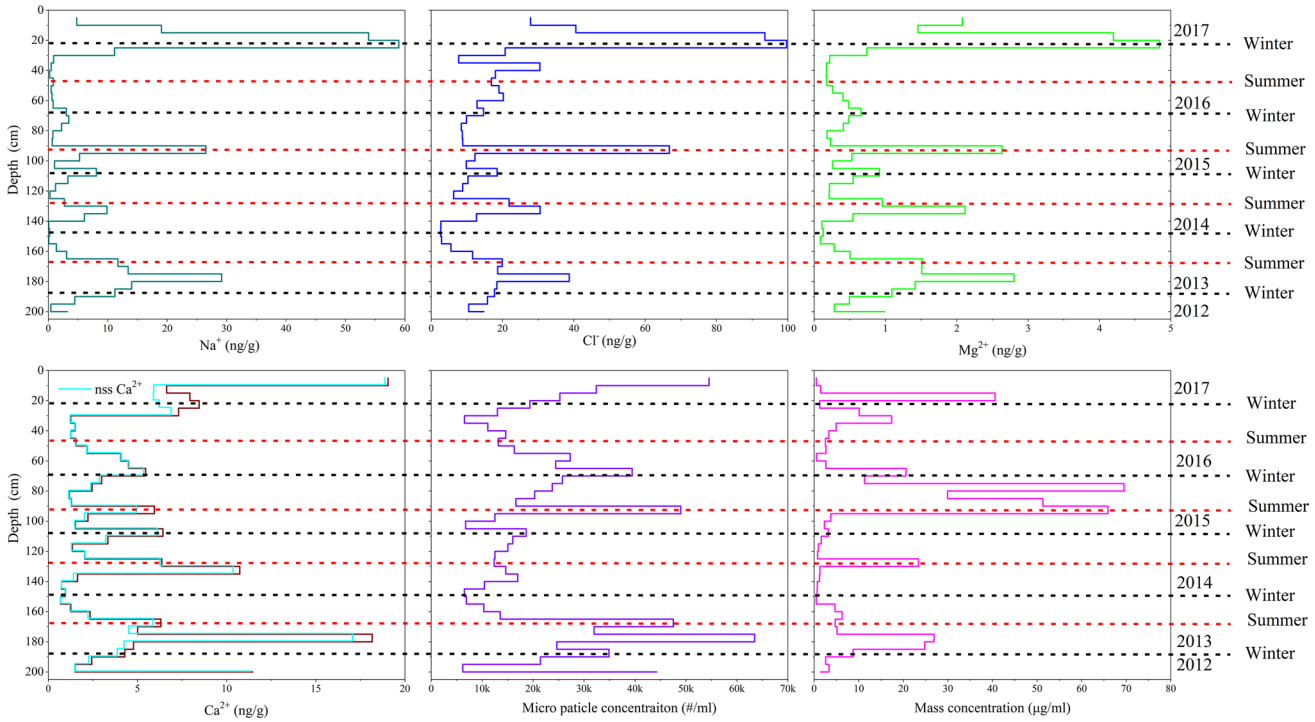

Fig. 3 Vertical profiles of the number of particles and the concentrations of mineral dust and ions (Na^+, Cl^-, Mg^{2+} and Ca^{2+} (nss Ca^{2+}))

the concentrations of the major ion species were observed. The concentrations of Na^+, NH_4^+, Mg^{2+}, Ca^{2+}, microparticles and dust exhibited annual peaks in the layers during the spring–winter seasons (Except 2015). The correlation matrices of all ion concentrations and microparticles are presented in Table 1. The seasonal variations were mainly traced using H/O isotopes ($\delta^{18}O$ and δD) and sea salt ions (Na^+, Cl^- and Mg^{2+}). The concentrations of non-sea salt Ca^{2+} (nss Ca^{2+}) were calculated with the equation [nss Ca^{2+}] = [Ca^{2+}]-(Ca^{2+}/Na^+)sea×[Na^+], where (Ca^{2+}/Na^+)sea uses the seawater ratio 0.038 (w/w) (Kang et al. 2015). The concentrations of nss Ca^{2+} ranged from 0.68 to 18.88 ng/g, with an average value of 4.21 ng/g.

The concentrations of MSA exhibited seasonal variations with the peak during summer, and the maximum values occurred in the summer-fall layers of the EGRIP snowpit (Fig. 4). The concentrations of NO_2^- and NO_3^- showed maximum peaks in summer, although another peak occasionally appeared in winter (Fig. 4). Multiple sources of sulfate aerosols were observed, including sea salt aerosols, volcanic activity, marine biogenic activity, mineral dust, and fossil fuel burning, which are usually influenced by complex chemical mechanisms (Legrand and Mayewski 1997). The nss SO_4^{2-} record showed significantly distinct variations in Na^+, Mg^{2+} and Ca^{2+} and Cl^-. The concentrations of nss SO_4^{2-} ranged from 6.3 to 353.9 ng/g, with a mean value of 70.7 ng/g and an average nss SO_4^{2-} of 96% (Fig. 4). The nss SO_4^{2-} reached a maximum (353.9 ng/g) in spring, 2015 because of the well-known Holuhraun eruption; thus, air pollutants produced by fossil fuel combustion can be excluded. In addition, the nss SO_4^{2-} record exhibited similar seasonal variations with MSA and presented maxima in the summer layers, indicating that dimethylsulfide (DMS) is also a predominant source of the SO_4^{2-}.

Discussion

Extreme climatic events based on hydrogen and oxygen stable isotopes

The D-excess values, which depend on the sea surface temperature and evaporation processes in the vapor source region (Masson-Delmotte et al. 2005), exhibit seasonal cycles but are not in phase with the $\delta^{18}O$ or δD variations. The D-excess peaks are shifted compared to those of $\delta^{18}O$ and δD, with the D-excess minimum occurring in spring-early summer (except 2012) and the D-excess maximum occurring in fall or winter season. The phase lag between D-excess and $\delta^{18}O$ and δD is affected by diffusion, with D-excess values driven by evaporation over the ocean, subsequent transportation to Greenland, and water vapor condensation when snow forms (Sodemann et al. 2008). Although $\delta^{18}O$ and δD in polar snow depend primarily on local temperatures, the D-excess in polar snow is largely influenced by the source temperature. In particular, the lower D-excess

Table 1 Pearson correlation matrix for ions and microparticles in the East GRIP snowpit. Bold entries indicate "strong" correlations

	Na^+	NH_4^+	Mg^{2+}	Ca^{2+}	MSA	Cl^-	F^-	NO_2^-	NO_3^-	SO_4^{2-}	nss SO_4^{2-}	nss Ca^{2+}	Microparticle
Na^+	1												
NH_4^+	0.390*	1											
Mg^{2+}	**0.949** **	**0.481** **	1										
Ca^{2+}	**0.469** **	0.402*	**0.668** **	1									
MSA	−0.146	0.084	−0.023	0.196	1								
Cl^-	**0.935** **	**0.511** **	**0.919** **	**0.464** **	−0.044	1							
F^-	0.139	**0.591** **	0.175	0.176	0.012	0.158	1						
NO_2^-	0.195	0.417**	0.246	0.415**	−0.070	0.207	0.000	1					
NO_3^-	0.037	**0.585** **	0.178	0.288	0.112	0.310	0.209	0.369*	1				
SO_4^{2-}	−0.027	0.059	0.004	0.004	0.190	−0.026	**0.513** **	−0.277	0.108	1			
nss SO_4^{2-}	−0.068	0.043	−0.035	−0.015	0.195	−0.065	**0.506** **	−0.284	0.106	**0.999** **	1		
nss Ca^{2+}	0.370*	0.375*	**0.586** **	**0.994** **	0.225	0.373*	0.168	0.413**	0.299	0.007	−0.008	1	
Microparticle	0.357*	**0.546** **	**0.501** **	**0.751** **	0.142	0.338*	0.308	**0.515** **	0.176	−0.063	−0.078	**0.746** **	1

* and ** represent significant at $P < 0.01$ and $P < 0.05$, respectively. $N = 40$

values during the winter seasons of 2014 and 2012 are consistent with the $\delta^{18}O$ and δD variations. Moreover, the large Holuhraun eruption occurred in 2014, which corresponded to lower $\delta^{18}O$ and δD values in 2014. The GrIS is a highly sensitive indicator of regional and global climate change, and has been undergoing rapidly warming since 2000, the extreme melting event occurred in 2012 across almost the entire surface (98.6% of the entire ice sheet surface) of the GrIS (Hanna et al. 2014). Therefore, these extreme events may have affected the abnormal D-excess values.

Efforts to understand the influence of historical global warming on individual extreme climate events have increased over the past decade. However, despite substantial progress, understanding events that are unprecedented in the local observational record remain a persistent challenge (Diffenbaugh et al. 2017). Temperatures in the Arctic are increasing two times as fast as the global average (Graham et al. 2017). The most rapid Arctic warming has been recorded during the winter months (Boisvert and Stroeve 2015; Graversen et al. 2008). Winter 2015–2016 featured an Arctic-wide (north of 66°N) winter temperature anomaly of approximately 5 °C, which was 2 °C warmer than the previous record (Overland and Wang 2016; Kim et al. 2017a, b). During this event, a strong intrusion of warm and moist air, an increase in downward longwave radiation and a loss of sea ice in the Barents and Kara seas were observed (Kim et al. 2017a, b). Observational analyses revealed that the abrupt warming was triggered by the entry of a strong Atlantic windstorm into the Arctic in late December 2015, which brought enormous moist and warm air masses (Kim et al. 2017a, b). In addition, an extremely cold event was recorded in the EGRIP snowpit in early spring 2017. The shifting of the polar vortex states may account for most of the recent winter cooling trends over some high-altitude regions via stratosphere–troposphere coupling (Kretschmer et al. 2017).

Environmental signals viewed from dust and ions seasonal variations

The continental source indicators of Ca^{2+}, microparticles and dust mass are consistent with that of sea salt ions. These results indicate that the main sources are sea salt ions from seawater from summer-autumn and the mineral dust originates from the low-latitude potential dust sources during spring. This result is supported by previous findings (Groot Zwaaftink et al. 2016); that is, mineral dust deposition from local sources peaks in autumn while dust deposition from remote sources peaks in spring. The average nss Ca^{2+} was 95%, indicating that there is a major source of nss Ca^{2+} carrying the mineral dust input via atmospheric transport from local or low-latitude dust source regions. Dust layers have been observed in spring layers over wide areas of the GrIS (Kang et al. 2015). Three maximum peaks were recorded

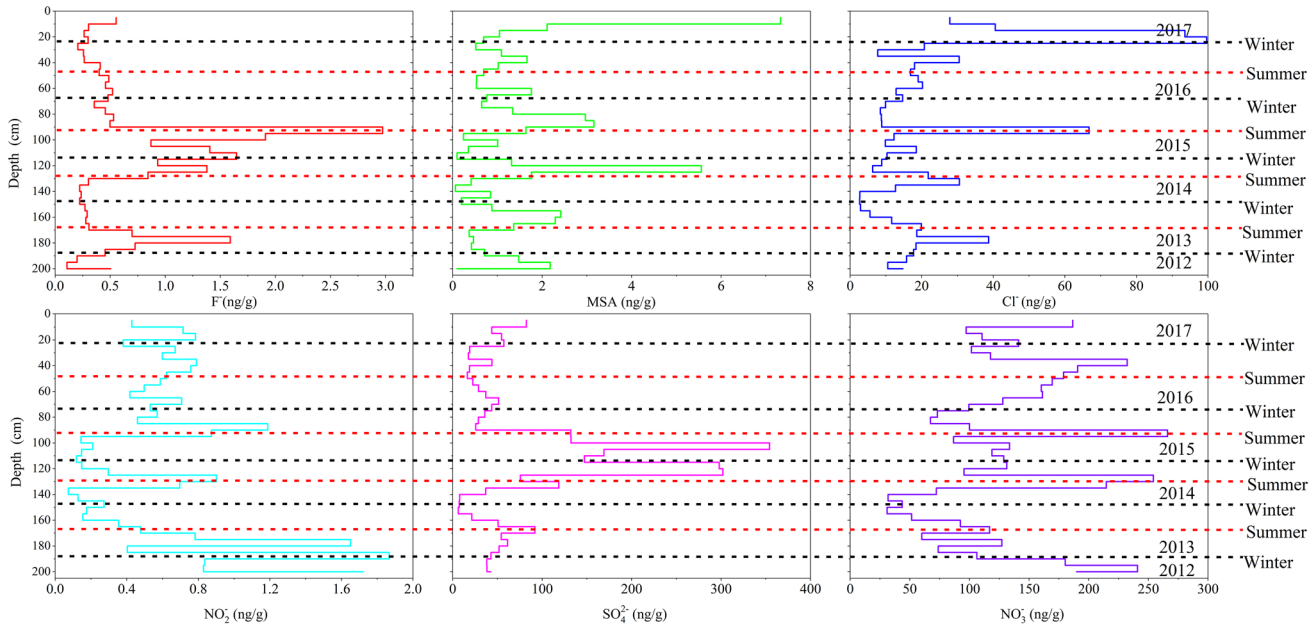

Fig. 4 Concentrations of anions (F^-, MSA, Cl^-, NO_2^-, SO_4^{2-} and NO_3^-) in the EGRIP snowpit

during the springs of 2013, 2015 and 2017. The location of this snowpit is approximately 1000 km downstream of the outlet glaciers (Vallelonga et al. 2014). Therefore, nss Ca^{2+} is expected to be abundant. Although data do not indicate the potential dust source in this region, previous studies have demonstrated that the large deserts and arid areas in Asia, such as the Taklimakan and Gobi deserts, could be natural dust sources for the GrIS (Újvári et al. 2015; Bory et al. 2014).

The concentrations of Na^+ and Cl^- in polar snow and ice are used as sea salt aerosol proxies because they originate primarily from sea spray aerosols (Legrand and Mayewski 1997). The correlation coefficient between Na^+ and Cl^- is 0.874 ($p < 0.01$) due to their identical marine provenances. The Na^+ and Cl^- in our snowpit exhibit seasonal variations with high concentrations in the winter–spring layers (Fig. 4). This phenomenon is consistent with previous result in the NEEM snowpit (Kang et al. 2015). The maximum peak of the Cl^-/Na^+ ratio occurred in summer of 2016, which supports a contribution of Cl^- derived from seawater because of the extremely warm event, and the sea ice area was greatly reduced in this year. Mg^{2+} and Ca^{2+} are commonly used as mineral dust proxies and indicate winter–spring seasonal dust variations (Kuramoto et al. 2011). Ca^{2+} (nss Ca^{2+}) seasonal variations in the East Greenland snowpit showed that these ions have the same continental dust source (Fig. 3; Table 1).

MSA is an important atmospheric oxidation product of dimethyl sulfide, and it is produced by marine biogenic activity and indicative of the sea ice extent (O'Dwyer et al. 2000). The seasonal cycle of MSA is dominantly influenced by marine biogenic activities. From spring to summer, marine phytoplankton, marine algae, and benthic diatoms begin to produce DMS, which is rapidly oxidized by hydroxyl and halogen radicals in the atmosphere and yields MSA and SO_2 (Legrand and Mayewski 1997). These seasonal variations are consistent with the changes in atmospheric MSA concentrations from the northwest GrIS (Kuramoto et al. 2011). High MSA concentrations were observed in the 2014 and 2017 summer layers, suggesting that higher temperatures (higher $\delta^{18}O$ and δD) and low sea ice occurred in both years. The nss SO_4^{2-} signal peaked in 2014, reflecting the well-known 2014 Holuhraun eruption. The maximum concentration of nss SO_4^{2-} was 353.9 ng/g, which is approximately 4–56 times greater than that in other years. No lag was observed between the eruption and the initial nss SO_4^{2-}deposition, which is consistent with the transport time of volcanic aerosols from the known eruption date (31 August 2014). An average 60,000 tonnes/day of SO_2 was released into the atmosphere, which affected the chemical composition of the rain, snow, and surface water; thus, the 2014/15 Bárðarbunga volcanic eruption was the largest in Iceland for more than 200 years after the eruption of Baroarbunga's Lakifissure in 1783 (Galeczka et al. 2016). Specifically, the high nss SO_4^{2-} concentration corresponds to the lowest values of $\delta^{18}O$ and δD, suggesting that a significant short-term cooling effect occurred during this eruption. This eruption record provides clues that can be used to reconstruct the history of eruptions in Iceland over much longer timescales.

Holuhraun eruption and transport paths

Volcanic eruptions can produce a considerable amount of acidic material (mainly H_2SO_4 but also halogenated gases, such as HF, HCl or HBr), and the acid content of ash is not trivial because this material can include H_2S, NH_3 and CH_4 (Halmer et al. 2002). A short fissure eruption occurred at the site of the pre-existing Holuhraun lavas on 29 August, and it lasted for approximately 5 h and produced less than 1 million m^3 of lava before the onset of the main basaltic effusive eruption on 31 August. Over the next 6 months, a 1.4–1.5 km^3 and 86 km^2 lava field was produced before the eruption ended on 27 February 2015 (Pedersen et al. 2017; Schmidt et al. 2015). In addition, river monitoring indicated that the dissolution of volcanic gases increased the SO_4^{2-}, F^-, and Cl^- concentrations in the local surface waters by up to two orders of magnitude, thereby decreasing the carbon alkalinity (Galeczka et al. 2016). Melted snow samples collected at the eruption site were characterized by a strong dependence of the pH on SO_4^{2-}, F^- and Cl^-, indicating that volcanic gases and aerosols acidified the snow (Galeczka et al. 2016).

The concentrations of F^- and NH_4^+ have increased significantly since autumn 2014. The concentrations of F^- and NH_4^+ also reached maximum values in spring 2014/2015 and were associated with peaks of nss SO_4^{2-} (Fig. 5). These records indicate that gas emissions (including HF and NH_3) were a primary component in this eruption. Why high concentrations of NO_3^- occurred during the autumn season of 2012 is unclear. The variations in NO_3^- in 2014/2015 show that the Holuhraun eruption was accompanied by a decrease in NO_3^-. Similar phenomena have been found in previous studies on Antarctic and Greenland ice cores (Röthlisberger et al. 2000; Clausen et al. 1997). Two possibilities were proposed by Röthlisberger et al. (2000) to explain this phenomenon. First, after a volcanic eruption, large amounts of SO_2 are emitted into the atmosphere, which will reduce the concentration of oxidants in the atmosphere and result in a decreased formation of NO_3^-. Another explanation is the mobilization of the ions occurring in snow and ice. A similar explanation was proposed by Wolff (1995), who suggested that when sulfate is deposited into snow, NO_3^- is mobilized and pushed to the sides of the SO_4^{2-} peak after recrystallization, leaving a NO_3^- decrease that coincides with the H_2SO_4 peak and slightly increased NO_3^- concentrations on the shoulders of the H_2SO_4 peak. This variation can be demonstrated in the EGRIP snowpit.

The nss SO_4^{2-} layer at the depth of 90–130 cm is associated with an episode of increased Holuhraun eruption inputs. However, significant correlations are not observed between the nss SO_4^{2-} peaks and dust microparticles or mass concentrations (Fig. 5). As mentioned above, because the Holuhraun eruption released much more gas (SO_2) at the start of the event, the eruption was gas rich and ash poor. The volume of tephra produced during this eruption was not substantial (Galeczka et al. 2016). The maximum plume height close to the eruption site was in the range of 1–3 km above ground. Therefore, gases were more easily transported to the GrIS and deposited into the snow. Based on the Lagrangian particle dispersion model FLEXPART, a previous study

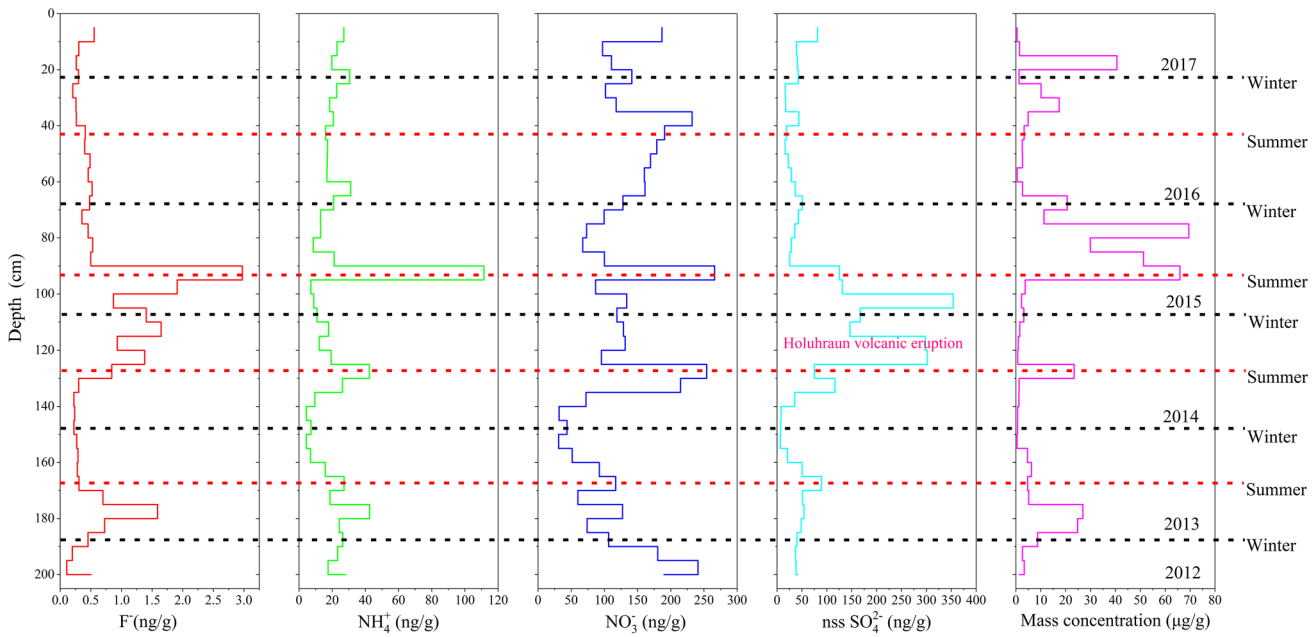

Fig. 5 Concentrations of F^-, NH_4^+, NO_3^- and nss SO_4^{2-} in the EGRIP snowpit

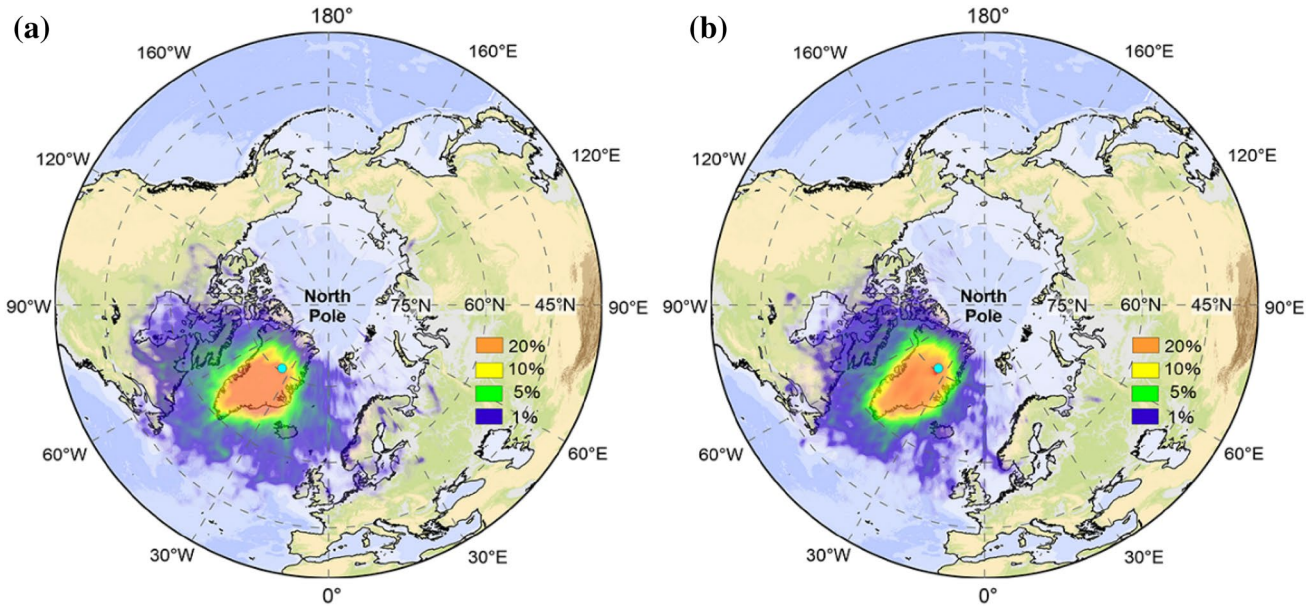

Fig. 6 Backward trajectories of air masses arriving at the EGRIP site from 2012 to 2017 **a** represents the winter–spring seasons and **b** represents the summer–autumn seasons)

indicated that approximately 6% of the dust deposited in the near-Arctic (> 60°N) was from Icelandic sources in the Arctic (Groot Zwaaftink et al. 2016). To obtain information on long distance sources of dust and anthropogenic pollutants during the sampling period, the HYSPLIT model was used. The seven-day backward trajectories were initialized every 6 h. The back-trajectory analysis for paths were at a low level (500 m AGL), and they were divided into winter–spring and summer–autumn seasons, which represented the dust and non-dust periods during 2012–2017, respectively. The Holuhraun fissure erupted on 31 August 2014, continued for 6 months, and officially ended on 28 February 2015. Therefore, this eruption mainly occurred in the winter season. Figure 6 shows that approximately 5–10% of the air mass from Iceland clearly arrived at the EGRIP snowpit. The air masses mainly originated from North America and Europe all the year. The air mass transporting paths are much more complicated during dust periods as observed in the effect from low latitudes, such as the Eurasian continent.

Conclusions

As part of an ongoing effort to develop impurity records at the EGRIP deep ice core, seasonal records of mineral dust and major ion concentrations were measured. Most of the ion concentrations showed maximum peaks during spring, which indicated that mineral dust originating from low altitudes was the main potential dust source. More importantly, our study revealed a well-known Holuhraun eruption event with high rates of F^-, $NH_4^+$and nss SO_4^{2-} and low rates of NO_3^- deposition from 31 August 2014 to 27 February 2015. Moreover, the lag of microparticle and dust mass concentrations (90 – 70 cm) compared with the nss SO_4^{2-} concentrations (135–85 cm) in the EGRIP snowpit indicated that this volcanic event was gas rich and ash (particle) poor and may indicate that SO_2 gas much more easily migrated to the bottom of the snow/ice by wet deposition. Therefore, these processes resulted in different layers between microparticle/dust and nss SO_4^{2-}concentrations in this snowpit. A back-trajectory analysis suggests that a major contributor to the Greenland aerosols (ash) was an air mass passing over Iceland. These results will contribute to an improved understanding of the snow chemistry of future deep EGRIP ice cores and provide additional clues to the mechanisms underlying the dramatic variations in the volcanic history of the GrIS in the future.

Acknowledgements This work was supported by the Strategic Priority Research Program of the Chinese Academy of Sciences (Grant No. XDA19070103), the National Natural Science Foundation of China (Grant No. 41425003; 41701071) and the CAS "Light of West China" Program.

Compliance with ethical standards

Conflict of interest The authors confirm that there are no conflicts of interest in this research.

References

Ambrose SH (1998) Late Pleistocene human population bottlenecks, volcanic winter, and differentiation of modern humans. J Hum Evol 34:623–651. https://doi.org/10.1006/jhev.1998.0219

Biscaye PE, Grousset FE, Revel M, Van der Gaast S, Zielinski GA, Vaars A, Kukla G (1997) Asian provenance of glacial dust (stage 2) in the Greenland Ice Sheet Project 2 ice core, Summit, Greenland. J Geophys Res 102:26765–26781. https://doi.org/10.1029/97JC01249

Boisvert LN, Stroeve JC (2015) The Arctic is becoming warmer and wetter as revealed by the Atmospheric Infrared Sounder. Geophys Res Lett 42:4439–4446. https://doi.org/10.1002/2015GL063775

Bory AJM, Abouchami W, Galer SJG, Svensson A, Christensen JN, Biscaye PE (2014) A chinese imprint in insoluble pollutants recently deposited in central greenland as indicated by lead isotopes. Environ Sci Technol 48:1451–1457. https://doi.org/10.1021/es4035655

Clausen HB, Hammer CU, Hvidberg CS, Dahl-Jensen D, Steffensen JP, Kipfstuhl J, Legrand M (1997) A comparison of the volcanic records over the past 4000 years from the Greenland Ice Core Project and Dye3 Greenland ice cores. J Geophys Res 102:26707–26723. https://doi.org/10.1029/97JC00587

Cole-Dai J, Ferris D, Lanciki A, Savarino J, Baroni M, Thiemens MH (2009) Cold decade (AD 1810–1819) caused by Tambora (1815) and another (1809) stratospheric volcanic eruption. Geophys Res Lett 36:L22703. https://doi.org/10.1029/2009GL040882

Diffenbaugh NS, Singh D, Mankin JS, Horton DE, Swain DL, Touma D, Charland A, Liu Y, Haugen M, Tsiang M, Rajaratnam B (2017) Quantifying the influence of global warming on unprecedented extreme climate events. Proc Nat Acad Sci 114:4881–4886. https://doi.org/10.1073/pnas.1618082114

Dong Z, Kang S, Qin D, Li Y, Wang X, Ren J, Li X, Yang J, Qin X (2016) Provenance of cryoconite deposited on the glaciers of the Tibetan Plateau: New insights from Nd-Sr isotopic composition and size distribution. J Geophys Res 121:7371–7382. https://doi.org/10.1002/2016JD024944

Drab E, Gaudichet A, Jaffrezo JL, Colin JL (2002) Mineral particles content in recent snow at Summit (Greenland). Atmos Environ 36:5365–5376. https://doi.org/10.1016/S1352-2310(02)00470-3

Fischer H, Siggaard Andersen ML, Ruth U, Röthlisberger R, Wolff E (2007) Glacial/interglacial changes in mineral dust and sea -salt records in polar ice cores: sources, transport, and deposition. Rev Geophys 45:1. https://doi.org/10.1029/2005RG000192

Fuhrer K, Wolff EW, Johnsen SJ (1999) Timescales for dust variability in the greenland ice core project (GRIP) ice core in the last 100,000 years. J Geophys Res 104:31043–31052. https://doi.org/10.1029/1999JD900929

Galeczka I, Sigurdsson G, Eiriksdottir ES, Oelkers EH, Gislason SR (2016) The chemical composition of rivers and snow affected by the 2014/2015 Bárðarbunga eruption, Iceland. J Volcanol Geother Res 316:101–119. https://doi.org/10.1016/j.jvolgeores.2016.02.017

Graham RM, Cohen L, Petty AA, Boisvert LN, Rinke A, Hudson SR, Nicolaus M, Granskog MA (2017) Increasing frequency and duration of Arctic winter warming events. Geophys Res Lett 44:6974–6983. https://doi.org/10.1002/2017GL073395

Graversen RG, Mauritsen T, Tjernström M, Källén E, Svensson G (2008) Vertical structure of recent Arctic warming. Nature 451:53. https://doi.org/10.1038/nature06502

Groot Zwaaftink CD, Grythe H, Skov H, Stohl A (2016) Substantial contribution of northern high-latitude sources to mineral dust in the Arctic. J Geophys Res 121:13, 613–678. https://doi.org/10.1002/2016JD025482. 697.

Halmer MM, Schmincke HU, Graf HF (2002) The annual volcanic gas input into the atmosphere, in particular into the stratosphere: a global data set for the past 100 years. J Volcanol Geoth Res 115:511–528. https://doi.org/10.1016/S0377-0273(01)00318-3

Hanna E, Fettweis X, Mernild SH, Cappelen J, Ribergaard MH, Shuman CA, Steffen K, Wood L, Mote TL (2014) Atmospheric and oceanic climate forcing of the exceptional Greenland ice sheet surface melt in summer 2012. Int J Climatol 34:1022–1037. https://doi.org/10.1002/joc.3743

Kang JH, Hwang H, Hong SB, Hur SD, Choi SD, Lee J, Hong S (2015) Mineral dust and major ion concentrations in snowpit samples from the NEEM site. Greenland Atmos Environ 120:137–143. https://doi.org/10.1016/j.atmosenv.2015.08.062

Kim BM, Hong JY, Jun SY, Zhang X, Kwon H, Kim SJ, Kim JH, Kim SW, Kim HK (2017a) Major cause of unprecedented Arctic warming in january 2016: critical role of an Atlantic windstorm. Sci Rep-Uk 7:40051. https://doi.org/10.1038/srep40051

Kim J, Kug J, Jeong S, Huntzinger DN, Michalak AM, Schwalm CR, Wei Y, Schaefer K (2017b) Reduced North American terrestrial primary productivity linked to anomalous Arctic warming. Nat Geosci 2017, 10(8):572–576. https://doi.org/10.1038/ngeo2986

Kretschmer M, Coumou D, Agel L, Barlow M, Tziperman E, Cohen J (2017) More-Persistent weak stratospheric polar vortex states linked to cold extremes. B Am Meteorol Soc. https://doi.org/10.1175/BAMS-D-16-0259.1

Kuramoto T, Gotoazuma K, Hirabayashi M, Miyake T, Motoyama H, Dahljensen D, Steffensen JP (2011) Seasonal variations of snow chemistry at NEEM, Greenland. Ann Glaciol 52:193–200. https://doi.org/10.3189/172756411797252365

Larsen LB, Vinther BM, Briffa KR, Melvin TM, Clausen HB, Jones PD, Siggaard-Andersen ML, Hammer CU, Eronen M, Grudd H, Gunnarson BE, Hantemirov RM, Naurzbaev MM, Nicolussi K (2008) New ice core evidence for a volcanic cause of the A.D. 536 dust veil. Geophys Res Lett. https://doi.org/10.1029/2007GL032450

Legrand M, Mayewski P (1997) Glaciochemistry of polar ice cores: a review. Rev Geophys 35:219–243. https://doi.org/10.1029/96RG03527

Li C, Kang S, Shi G, Huang J, Ding M, Zhang Q, Zhang L, Guo J, Xiao C, Hou S, Sun B, Qin D, Ren J (2014) Spatial and temporal variations of total mercury in Antarctic snow along the transect from Zhongshan Station to Dome A. Tellus B: Chemical and Physical Meteorology. 66:25152. https://doi.org/10.3402/tellusb.v66.25152

Masson-Delmotte V, Jouzel J, Landais A, Stievenard M, Johnsen SJ, White JWC, Werner M, Sveinbjornsdottir A, Fuhrer K (2005) GRIP Deuterium Excess Reveals Rapid and Orbital-Scale changes in greenland moisture origin. Science 309:118–121. https://doi.org/10.1126/science.1108575

Mayewski PA, Meeker LD, Morrison MC, Twickler MS, Whitlow SI, Ferland KK, Meese DA, Legrand MR, Steffensen JP (1993) Greenland ice core "signal" characteristics: An expanded view of climate change. J Geophys Res 98:12839–12847. https://doi.org/10.1029/93JD01085

McConnell JR, Edwards R (2008) Coal burning leaves toxic heavy metal legacy in the Arctic. Proc Nat Acad Sci 105:12140–12144. https://doi.org/10.1073/pnas.0803564105

O'Dwyer J, Isaksson E, Vinje T, Jauhiainen T, Moore J, Pohjola V, Vaikmäe R, Wal RS, WV (2000) Methanesulfonic acid in a Svalbard Ice Core as an indicator of ocean climate. Geophys Res Lett 27:1159–1162. https://doi.org/10.1029/1999GL011106

Overland JE, Wang M (2016) Recent extreme arctic temperatures are due to a split polar vortex. J Climate 29:5609–5616. https://doi.org/10.1175/JCLI-D-16-0320.1

Oyabu I, Iizuka Y, Fischer H, Schüpbach S, Gfeller G, Svensson A, Fukui M, Steffensen JP, Hansson M (2015) Chemical compositions of solid particles present in the Greenland NEEM ice core

over the last 110,000 years. J Geophys Res 120:9789–9813. https://doi.org/10.1002/2015JD023290

Pedersen GBM, Höskuldsson A, Dürig T, Thordarson T, Jónsdóttir I, Riishuus MS, Óskarsson BV, Dumont S, Magnusson E, Gudmundsson MT, Sigmundsson F, Drouin VJPB, Gallagher C, Askew R, Gudnason J, Moreland WM, Nikkola P, Reynolds HI, Schmith J (2017) Lava field evolution and emplacement dynamics of the 2014–2015 basaltic fissure eruption at Holuhraun. Iceland J Volcanol Geoth Res 340:155–169. https://doi.org/10.1016/j.jvolgeores.2017.02.027

Ram M, Stolz M, Koenig G (1997) Eleven year cycle of dust concentration variability observed in the dust profile of the GISP2 Ice core from central Greenland: Possible solar cycle connection. Geophys Res Lett 24:2359–2362. https://doi.org/10.1029/97GL02521

Robock A (2000) Volcanic eruptions and climate. Rev Geophys 38:191–219. https://doi.org/10.1029/1998RG000054

Röthlisberger R, Bigler M, Hutterli M, Sommer S, Stauffer B, Junghans HG, Wagenbach D (2000) Technique for continuous high-resolution analysis of trace substances in firn and ice cores. Environ Sci Technol 34:338–342. https://doi.org/10.1021/es9907055

Ruth U, Wagenbach D, Steffensen JP, Bigler M (2003) Continuous record of microparticle concentration and size distribution in the central Greenland NGRIP ice core during the last glacial period. J Geophys Res 108. https://doi.org/10.1029/2002JD002376

Schmidt A, Leadbetter S, Theys N, Carboni E, Witham CS, Stevenson JA, Birch CE, Thordarson T, Turnock S, Barsotti S, Delaney L, Feng W, Grainger RG, Hort MC, Höskuldsson Á, Ialongo I, Ilyinskaya E, Jóhannsson T, Kenny P, Mather TA, Richards NAD, Shepherd J (2015) Satellite detection, long-range transport, and air quality impacts of volcanic sulfur dioxide from the 2014–2015 flood lava eruption at Bárðarbunga (Iceland). J Geophys Res 120:9739–9757. https://doi.org/10.1002/2015JD023638

Sigl M, McConnell JR, Layman L, Maselli O, McGwire K, Pasteris D, Dahl Jensen D, Steffensen JP, Vinther B, Edwards R (2013) A new bipolar ice core record of volcanism from WAIS Divide and NEEM and implications for climate forcing of the last 2000 years. J Geophys Res 118:1151–1169. https://doi.org/10.1029/2012JD018603

Sodemann H, Schwierz C, Wernli H (2008) Interannual variability of Greenland winter precipitation sources: Lagrangian moisture diagnostic and North Atlantic Oscillation influence. J Geophys Res. https://doi.org/10.1029/2007JD008503

Steffensen JP (1997) The size distribution of microparticles from selected segments of the Greenland Ice Core Project ice core representing different climatic periods. J Geophys Res 102:26755–26763. https://doi.org/10.1029/97JC01490

Újvári G, Stevens T, Svensson A, Klötzli US, Manning C, Németh T, Kovács J, Sweeney MR, Gocke M, Wiesenberg GL (2015) Two possible source regions for central Greenland last glacial dust. Geophys Res Lett. https://doi.org/10.1002/2015GL066153

Vallelonga P, Christianson K, Alley RB, Anandakrishnan S, Christian JEM, Dahl-Jensen D, Gkinis V, Holme C, Jacobel RW, Karlsson NB, Keisling BA, Kipfstuhl S, Kjær HA, Kristensen MEL, Muto A, Peters LE, Popp T, Riverman KL, Svensson AM, Tibuleac C, Vinther BM, Weng Y, Winstrup M (2014) Initial results from geophysical surveys and shallow coring of the Northeast Greenland Ice Stream (NEGIS). Cryosphere. 8:1275–1287. https://doi.org/10.5194/tc-8-1275-2014, 2014

Williams MAJ, Ambrose SH, van der Kaars S, Ruehlemann C, Chattopadhyaya U, Pal J, Chauhan PR (2009) Environmental impact of the 73 ka Toba super-eruption in South Asia. Palaeogeogr Palaeoclimatol Palaeoecol 284:295–314. https://doi.org/10.1016/j.palaeo.2009.10.009

Wolff EW (1995) Nitrate in Polar Ice. Ice core studies of global biogeochemical cycles. Springer, Berlin, 1995. 195–224